
N-Acetylcysteine– and MK-801–Induced Changes in Glutamate Levels Do Not Affect In Vivo Binding of Metabotropic Glutamate 5 Receptor Radioligand ¹¹C-ABP688 in Rat Brain

Tine Wyckhuys¹, Jeroen Verhaeghe¹, Leonie Wyffels², Xavier Langlois³, Mark Schmidt³, Sigrid Stroobants^{1,2}, and Steven Staelens¹

¹Molecular Imaging Center Antwerp, University of Antwerp, Antwerp, Belgium; ²Nuclear Medicine, University Hospital Antwerp, Antwerp, Belgium; and ³Department of Neuroscience, Janssen Pharmaceutica NV, Beerse, Belgium

Abnormal glutamate transmission is involved in various neurologic disorders, such as epilepsy, schizophrenia, and Parkinson disease. At present, no imaging techniques are capable of measuring acute fluctuations in endogenous glutamate levels in vivo. We evaluated the potential of ¹¹C-ABP688, a PET ligand that binds to an allosteric site of the metabotropic glutamate 5 receptor, in rats by using small-animal PET and β -microprobes after pharmacologic challenges with *N*-acetylcysteine (NAC) and MK-801. Both compounds are known to induce increases in endogenous glutamate levels.

Methods: Three experiments with ¹¹C-ABP688 were performed to validate our study setup: first, metabolite analyses during workup ($n = 3$) and after a selected treatment ($n = 3$); second, a test–retest ($n = 12$) small-animal PET experiment (1 h scan; 27.75 MBq of ¹¹C-ABP688 administered intravenously; <3 nmol/kg); and third, a small-animal PET and β -microprobe cold blocking study ($n = 6$ /condition) with unlabeled ABP688. After this experimental validation, rats were pretreated with either NAC (intravenous infusion of 50 mg/kg/h) or MK-801 (0.16 mg/kg; given intraperitoneally); this step was followed by small-animal PET with ¹¹C-ABP688 ($n = 12$) or β -microprobe measurements ($n = 10$ /condition) of ¹¹C-ABP688. Time–activity curves were extracted, and the nondisplaceable binding potential (BP_{ND}) was calculated by use of the simplified reference tissue model with the cerebellum as a reference region.

Results: ¹¹C-ABP688 BP_{ND} measurements were highly reproducible (test–retest), and both small-animal PET and β -microprobes were able to discriminate changes in ¹¹C-ABP688 binding (cold blocking). The average small-animal PET BP_{ND} measurements in the test experiment for the caudate putamen, frontal cortex, cerebral cortex, hippocampus, and thalamus were 2.58, 1.40, 1.60, 1.86, and 1.09, respectively. However, no significant differences in BP_{ND} measurements were observed with small-animal PET in the test and retest conditions on the one hand and the NAC and MK-801 conditions on the other hand for any of these regions. When β -microprobes were used, the average BP_{ND} in the caudate putamen was 0.94, and no significant changes in the test and MK-801 conditions were observed. **Conclusion:** Pharmacologic challenges with NAC and MK-801 did not affect the ¹¹C-ABP688 BP_{ND} in the rat brain. These data suggest that the in vivo affinity of ¹¹C-ABP688 for binding to an allosteric site of the metabotropic

glutamate 5 receptor is not modulated by changes in glutamate levels and that ¹¹C-ABP688 is not capable of measuring acute fluctuations in endogenous levels of glutamate in vivo in the rat brain.

Key Words: small-animal PET; β -microprobes; binding potential; glutamate; mGluR5

J Nucl Med 2013; 54:1954–1961

DOI: 10.2967/jnumed.113.121608

Glutamate is the most abundant excitatory neurotransmitter of the nervous system. Abnormal glutamate neurotransmission has been implicated in the pathophysiology of various neurologic disorders, such as epilepsy (1), schizophrenia (2), and Parkinson disease (3). As a result, intervention through the glutamate system has become the target of multiple lines of research. At present, no imaging techniques are capable of measuring acute fluctuations in endogenous levels of glutamate in vivo, partly because of the lack of dedicated (radio)tracers. Recently, the visualization of acute fluctuations in endogenous glutamate levels was suggested (4) in a study performed in baboons with PET and the radioligand ¹¹C-ABP688 [3-(6-methyl-pyridin-2-ylethynyl)-cyclohex-2-enone-*O*-¹¹C-methyloxime], a highly selective allosteric antagonist of the metabotropic glutamate 5 receptor (mGluR5) (5). In that study (4), a significant decrease in ¹¹C-ABP688 binding relative to that at the baseline was observed in relevant brain regions after pharmacologic challenge with *N*-acetylcysteine (NAC). NAC is known to indirectly increase extrasynaptic glutamate release through activation of the cystine–glutamate antiporter (6,7). The findings of that study (4) suggested that a glutamate receptor PET tracer could be used to measure changes in glutamate levels in vivo, and it was hypothesized that the NAC-induced increase in extrasynaptic glutamate produced a shift in the affinity of binding of the ¹¹C-ABP688 tracer to an allosteric site of mGluR5. In the present study, we attempted to confirm these findings in the rat brain by using small-animal PET and β -microprobes after pretreatments with NAC and MK-801.

¹¹C-ABP688 can exist in 2 stereoisomeric forms; the (*E*)-isomer (referred to here as ¹¹C-ABP688) is the most potent (5). To evaluate the in vivo stability of the ¹¹C-ABP688 tracer and possible isomerization, we performed an in vivo metabolite study during

Received Feb. 20, 2013; revision accepted Jun. 20, 2013.
For correspondence or reprints contact: Steven Staelens, Molecular Imaging Center Antwerp, Universiteitsplein 1, 2610 Wilrijk, Belgium.
E-mail: Steven.Staelens@uantwerpen.be
Published online Sep. 19, 2013.
COPYRIGHT © 2013 by the Society of Nuclear Medicine and Molecular Imaging, Inc.

work-up and after an MK-801 challenge. Further, to validate our small-animal PET setup with ^{11}C -ABP688, we performed both a test–retest study ($n = 12$) and a blocking study ($n = 6$) with unlabeled ABP688 by using a volume-of-interest (VOI) analysis in delineated structures that show specific ^{11}C -ABP688 binding: caudate putamen, frontal cortex, cerebral cortex, hippocampus, and thalamus (8,9). The cerebellum is a suitable reference region for calculating the nondisplaceable binding potential (BP_{ND}) of ^{11}C -ABP688 in rats and nonhuman primates (4,8), allowing for noninvasive quantification with the simplified reference tissue model (8,9). Because of the limited spatial resolution and partial-volume effects of small-animal PET, additional experiments with β -microprobes were also executed. β -microprobes—radiosensitive probes implanted stereotactically in anesthetized animals—record real-time kinetics of positron emitters within a few millimeters around the tip of the probe (10). To validate our β -microprobe setup with ^{11}C -ABP688, we implanted β -microprobes in the caudate putamen and cerebellum of untreated animals ($n = 6$); we also performed a blocking study with unlabeled ABP688 ($n = 6$).

Next, endogenous glutamate levels were increased in vivo through a pharmacologic challenge with NAc, a cysteine derivative, and evaluated with small-animal PET. Both small-animal PET scans and β -microprobe measurements were obtained after the injection of MK-801, an *N*-methyl-*D*-aspartate (NMDA) receptor antagonist. Both NAc (6) and MK801 (11) are known to increase extraneuronal glutamate levels.

MATERIALS AND METHODS

Animals

Sprague–Dawley rats (Charles River Laboratories) weighing 275–350 g were treated in accordance with the European Ethics Committee (decree 86/609/CEE), and the study protocol was approved by the Animal Experimental Ethical Committee of the University of Antwerp, Antwerp, Belgium (2011-67). The animals were kept in individually ventilated cages under environmentally controlled conditions (12-h normal light–dark cycles, 20°C–23°C, and 50% relative humidity) with food and water ad libitum.

Pharmaceuticals

Pharmacologic challenges were performed with the following pharmaceuticals: unlabeled ABP688 dissolved in a mixture of polyethylene glycol 200 and saline (50:50) (12), NAc (*N*-acetyl-L-cysteine; Sigma Aldrich; 50 mg/kg) dissolved in saline, and MK-801 [(+)-MK-

801 hydrogen maleate; Sigma Aldrich; 0.16 mg/kg] dissolved in saline.

Radiosynthesis

^{11}C -ABP688 was prepared by reaction of 0.5 mg of desmethyl-ABP688 (*E,Z*) with ^{11}C - $\text{CH}_3\text{SO}_3\text{CF}_3$ in 400 μL of acetone in the presence of 10 μL of 1N NaOH for 4 min at room temperature. For purification, the crude reaction mixture was injected into an analytical high-performance liquid chromatography (HPLC) column (Waters X-Bridge C18; 5 μm ; 4.6 \times 150 mm) with an eluent of 0.05 M sodium acetate (pH 5.5) and ethanol (55:45, v/v) at a flow rate of 1 mL/min to isolate (*E*)- ^{11}C -ABP688. Purified (*E*)- ^{11}C -ABP688 was filtered through a sterile Millipore Millex-GV filter (0.22 μm) and diluted with 0.9% NaCl through the same filter to reduce the ethanol concentration to less than 10%. The average specific activity, injected dose, and injected mass for each experiment are shown in Table 1; the injected volume of ^{11}C -ABP688 was 0.5 mL.

Experimental Protocols

First, to validate the extraction procedure and the stability of the tracer during work-up, we performed a metabolite analysis. Blood and brain tissues of rats ($n = 3$) were collected, spiked with ^{11}C -ABP688, and analyzed by HPLC and γ counting. Rats also were given either vehicle injection ($n = 3$) or MK-801 challenge (0.16 mg/kg; 0.16 mg/mL; given intraperitoneally) ($n = 3$). After this pretreatment, ^{11}C -ABP688 was injected, and rats were decapitated 60 min after tracer injection. Blood and brain tissues were collected, and the samples were further analyzed for the presence of metabolites.

Next, we performed test, retest, and NAc challenge small-animal PET studies. Rats ($n = 12$) were scanned on 3 different days under different pretreatment conditions in random order. The animals were anesthetized (1.5% isoflurane mixed with medical oxygen), positioned on the scanner, and given either vehicle (for both test and retest conditions) or NAc (7.5 mg/mL; 50 mg/kg/h; intravenously in the tail) infusion for 60 min. After this pretreatment, the infusion was stopped, ^{11}C -ABP688 was injected, and the small-animal PET scan was started.

Subsequently, a small-animal PET blocking experiment was performed. Rats were anesthetized (1.5% isoflurane mixed with medical oxygen), positioned on the scanner, and injected (intravenously in the tail) with various amounts of unlabeled ABP688. At 10 min after this injection, a bolus of ^{11}C -ABP688 was injected concurrently with the initiation of the small-animal PET acquisition. The various total amounts of unlabeled ABP688 (pretreatment plus tracer bolus) were as follows: vehicle (ABP688; 0.7 $\mu\text{g}/\text{kg}$; $n = 6$), 0.003 mg/kg (0.004 mg/mL; $n = 3$), 0.0098 mg/kg (0.02 mg/mL; $n = 3$), 0.018 mg/kg (0.04

TABLE 1
Specific Activity (SA) at Time of Injection and Injected Dose (ID) and Injected Mass (IM) per Experiment

| Study | Condition | Mean \pm SD | | |
|--|---------------------|----------------------------|-------------------|-----------------|
| | | SA (GBq/ μmol) | ID (MBq) | IM (nmol/kg) |
| Metabolite | Vehicle | 20.12 \pm 3.75 | 51.06 \pm 27.01 | 6.40 \pm 3.55 |
| | MK-801 | 22.55 \pm 8.30 | 79.18 \pm 28.12 | 9.32 \pm 1.66 |
| Test–retest and NAc challenge (small-animal PET) | Test | 25.65 \pm 4.24 | 27.75 \pm 5.92 | 3.06 \pm 0.27 |
| | Retest | 27.35 \pm 6.83 | 29.23 \pm 7.40 | 3.01 \pm 0.19 |
| | NAc | 25.84 \pm 6.03 | 27.75 \pm 5.55 | 3.06 \pm 0.28 |
| Blocking | Small-animal PET | 13.82 \pm 7.08 | 26.64 \pm 13.32 | 4.73 \pm 1.78 |
| | β -microprobe | 18.42 \pm 6.66 | 18.50 \pm 8.14 | 2.61 \pm 0.38 |
| MK-801 challenge (small-animal PET) | Vehicle | 19.59 \pm 4.61 | 23.31 \pm 5.55 | 2.87 \pm 0.22 |
| | MK-801 | 23.50 \pm 5.90 | 27.75 \pm 8.14 | 2.85 \pm 0.12 |
| MK-801 challenge (β -microprobe) | Vehicle | 13.82 \pm 6.10 | 15.54 \pm 8.51 | 2.86 \pm 0.43 |
| | MK-801 | 17.05 \pm 5.65 | 19.61 \pm 6.66 | 2.87 \pm 0.25 |

mg/mL; $n = 3$), 0.085 mg/kg (0.2 mg/mL; $n = 3$), 0.84 mg/kg (2 mg/mL; $n = 3$), and 3 mg/kg (2 mg/mL; $n = 6$).

This step was followed by a β -microprobe blocking experiment. Rats ($n = 6$ /condition) were anesthetized (1.5% isoflurane mixed with medical oxygen), implanted with 2 β -microprobes (1 in the caudate putamen and 1 in the cerebellum), and given either vehicle or unlabeled ABP688 (3 mg/kg; 2 mg/mL; intravenously in the tail). Next, ^{11}C -ABP688 was injected concurrently with the initiation of the β -microprobe measurements, and rats were decapitated 60 min after tracer injection.

Further, an MK-801 small-animal PET study was executed. Rats ($n = 12$) were anesthetized (1.5% isoflurane mixed with medical oxygen) and positioned on the scanner, and 2 scans were obtained in random order on 2 different days: 1 after intraperitoneal injection of vehicle and 1 after intraperitoneal pharmacologic challenge with MK-801 (0.16 mg/kg; 0.16 mg/mL). At 20 min after this pretreatment, ^{11}C -ABP688 was injected, and small-animal PET scanning was started.

Finally, an MK-801 β -microprobe experiment was performed. Rats ($n = 10$ /condition) were anesthetized (1.5% isoflurane mixed with medical oxygen), implanted with 2 β -microprobes, and injected intraperitoneally with vehicle or MK-801 (0.16 mg/kg; 0.16 mg/mL). Next, ^{11}C -ABP688 was injected concurrently with the initiation of the β -microprobe measurements, and rats were decapitated 60 min after tracer injection.

Techniques

For validation of the extraction procedure and the stability of the tracer during work-up, blood and brain samples were spiked with approximately 37 kBq of ^{11}C -ABP688. The blood was centrifuged for 3 min at 4,000 rpm and 4°C. Plasma (400 μL) was removed, and 400 μL of acetonitrile (ACN) and 10 μL of unlabeled ABP688 (*E,Z*) (1 mg/mL) were added for UV reference and nonspecific saturation. The brain was divided into 2 equal parts. Each part was homogenized in 1 mL of ACN and 10 μL of unlabeled ABP688 (*E,Z*) (1 mg/mL). The activity in the tubes was measured with an automated γ counter (Perkin Elmer). After 30 s of mixing, the brain and plasma mixtures were centrifuged for 5 min at 4,000 rpm and 4°C. The supernatant was separated from the precipitate, and the activities in both fractions were measured. During work-up, all samples were kept on ice. The extraction efficiency (percentage) was expressed as the ratio of the amount of radioactivity present in the supernatant to the total amount of radioactivity present in the plasma or brain sample.

The stability of the tracer during work-up was determined by analysis of 100 μL of supernatant from the spiked plasma and brain samples with an HPLC system (Waters X-Bridge C18; 5 μm ; 150 \times 4.6 mm), a guard column (SecurityGuard; Phenomenex), and a mixture of 0.05 M sodium acetate (pH 5.5) and ACN (50:50, v/v) as the mobile phase. The HPLC eluate was collected in fractions at 30 s, and their radioactivity was determined.

For evaluation of in vivo metabolism, after rats were decapitated, blood was collected in an ethylenediaminetetraacetic acid-coated tube and centrifuged for 3 min at 4,000 rpm and 4°C to separate the plasma. Next, the plasma (400 μL) was mixed with 400 μL of ACN, and the brain was homogenized in 2 mL of ACN. After 30 s of mixing, both the plasma and the homogenized brain were centrifuged for 5 min at 4,000 rpm and 4°C. Supernatants were collected and analyzed by HPLC as described earlier.

Small-animal PET specifications were as follows. Dynamic small-animal PET imaging (60 min; frames: 2 \times 10 s, 3 \times 20 s, 3 \times 30 s, 3 \times 60 s, 3 \times 150 s, and 9 \times 300 s) was performed with 2 Siemens Inveon PET/CT scanners (Siemens Preclinical Solution; IAW software version 1.5.0.28) (13–15). Animals were randomized to each of the scanners. An animal was then always scanned on the same scanner for each of its challenges. The temperature was kept constant during scanning.

For quantitative analysis, small-animal PET images were reconstructed by use of 2-dimensional ordered-subset expectation maximization (16) with 4 iterations and 16 subsets after Fourier rebinning (17). The PET images were reconstructed on a 128 \times 128 \times 159 grid with a pixel size of 0.776 \times 0.776 \times 0.776 mm. The reconstructed spatial resolution was about 1.4 mm at the center of the field of view (with filtered backprojection). Normalization, dead time correction, random subtraction, CT-based attenuation, and single-scatter simulation scatter corrections (18) were applied. For each dynamic acquisition, a static image corresponding to the time-averaged frames was spatially transformed through brain normalization with PMOD v3.3 (PMOD Technologies) to an in-house-developed ^{11}C -ABP688 template of the rat brain. Each frame in the dynamic sequence of individual scans was then transformed to the ^{11}C -ABP688 template space according to calculated transformation parameters. The time-activity curves for several VOIs (caudate putamen, 43.5 mm³; frontal cortex, 1.4 mm³; cerebral cortex, 26.3 mm³; hippocampus, 17.4 mm³; and thalamus, 30.7 mm³) were extracted from the images.

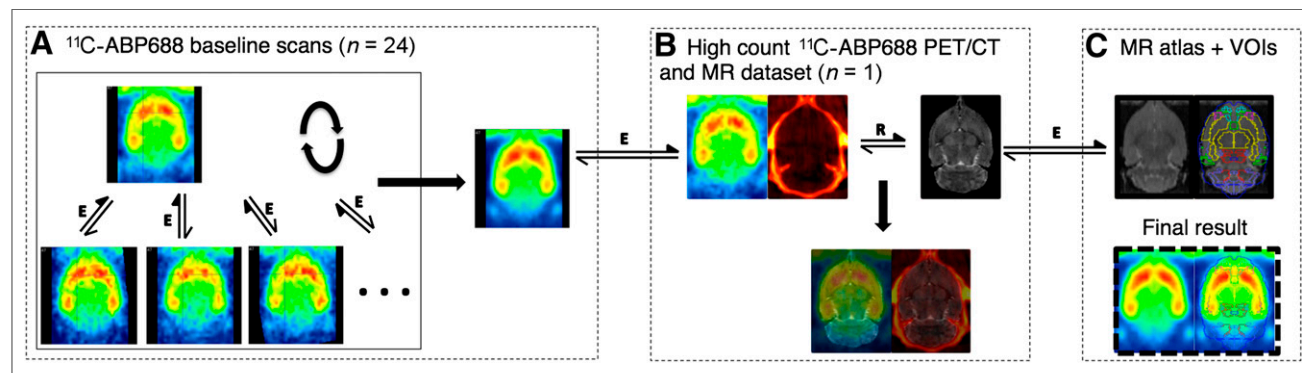


FIGURE 1. Creation of ^{11}C -ABP688 brain template in standardized MR space (Schiffer rat MR image atlas available in PMOD v3.3) and VOI definition. (A) Iterative averaging and registering of 24 baseline scans and 1 high-count ^{11}C -ABP688 scan to form average brain ^{11}C -ABP688 template. (B) Combining T2 MR image and high-count PET/CT image datasets allowed registering of PET images to MR images through rigid matching of MR and CT images. (C) Matching of MR image in B to MR image atlas through elastic registration. Through application of combined transformations, ^{11}C -ABP688 template in A could be transformed to standardized space in C, allowing use of predefined VOIs. Double-sided arrows indicate registration steps (E = elastic; R = rigid); filled arrows indicate reference images.

TABLE 2
 BP_{ND} and Absolute ΔBP_{ND} for Test, Retest, and NAc Challenges in ^{11}C -ABP688 Small-Animal PET

| Region | Mean \pm SD | | | | |
|-----------------|-----------------|------------------|------------------------------|-----------------|---------------------------|
| | Test BP_{ND} | Retest BP_{ND} | Test–retest ΔBP_{ND} | NAc BP_{ND} | Test–NAc ΔBP_{ND} |
| Caudate putamen | 2.58 \pm 0.28 | 2.52 \pm 0.23 | 2.0% \pm 10.7% | 2.54 \pm 0.17 | 1.2% \pm 10.7% |
| Frontal cortex | 1.40 \pm 0.12 | 1.42 \pm 0.14 | 1.0% \pm 11.1% | 1.42 \pm 0.12 | 1.3% \pm 11.1% |
| Cerebral cortex | 1.60 \pm 0.12 | 1.58 \pm 0.12 | 1.0% \pm 7.7% | 1.61 \pm 0.11 | 0.6% \pm 8.9% |
| Hippocampus | 1.86 \pm 0.17 | 1.85 \pm 0.14 | 0.6% \pm 9.9% | 1.88 \pm 0.16 | 0.9% \pm 9.6% |
| Thalamus | 1.09 \pm 0.16 | 1.07 \pm 0.10 | 1.5% \pm 15.6% | 1.08 \pm 0.12 | 0.6% \pm 17.6% |

The ^{11}C -ABP688 template was obtained as follows (Fig. 1). In 1 animal, both a high-resolution, 9.4 T T2 MR image and a high-count (51.8 MBq) ^{11}C -ABP688 small-animal PET/CT image were obtained with a specially designed animal holder. This holder allowed the automated rigid registration of the anatomic MR and CT images and the subsequent coregistration of the PET image to the MR image. The high-resolution MR image was then transformed to the Schiffer rat MR atlas available in PMOD v3.3 (PMOD brain normalization), which contains all of the delineated relevant brain VOIs. The 24 ^{11}C -ABP688 baseline static images from the test–retest experiment (12 test and 12 retest images) were first normalized to the high-count PET image, and then the 25 images were iteratively averaged and registered (3 iterations). The average aligned ^{11}C -ABP688 image could then be transformed into the PMOD rat brain VOI space through the CT and MR imaging transforms.

The BP_{ND} of ^{11}C -ABP688 for the different VOIs was then calculated by use of the simplified reference tissue model (19) with the cerebellum as a reference region (8,9). The percentage change in BP_{ND} across conditions (ΔBP_{ND}) was calculated as follows:

$$\Delta BP_{ND} = \frac{BP_{ND}(C2) - BP_{ND}(C1)}{\text{mean}(BP_{ND}(C1), BP_{ND}(C2))}$$

where $BP_{ND}(C1)$ represents the BP_{ND} in condition 1.

β -microprobe specifications were as follows. About 1.5 h before tracer injection, animals were anesthetized (1.5% isoflurane mixed with medical oxygen). As soon as deep anesthesia was obtained, animals were immobilized in the stereotactic frame (Kopf Instruments). After exposure of the skull, 2 holes were drilled for positioning of the probes in both the caudate putamen and the cerebellum. Anteroposterior and mediolateral coordinates are referenced from the

bregma, and dorsoventral coordinates are referenced from the skull. For the caudate putamen (20), the coordinates for implantation were as follows: anteroposterior, +0.2; mediolateral, 3.0; and dorsoventral, –6.0; for the cerebellum (21), the coordinates were as follows: anteroposterior, –11.8; mediolateral, 0.0; and dorsoventral, –3.5. Body temperature was maintained at 37°C throughout the experiment.

For the β -microprobe recordings, a Microscintillator twin-system (SwissTrace) was used together with 2 scintillator probes (0.5 mm) (22). The β -microprobe recorded the positrons (β^+ particles) emitted by the radiotracer. Recordings were acquired and corrected with the SwissTrace counter module in PMOD v3.0. Sampling was done at 1-s intervals. Before each recording, the photomultiplier tubes were allowed to warm up and stabilize for at least 30 min. After implantation with the 2 β -microprobes, the animals were injected with ^{11}C -ABP688. Recording was started at least 1 min before injection and continued for 1 h after injection. At the end of the experiment, the animals were injected with an overdose of pentobarbital (>30 mg/kg).

After this procedure, the animals were removed from the stereotactic apparatus, both probes were cleaned, and calibration of the probes was performed with an aqueous solution (10 mL) of ^{18}F -FDG (\approx 20 MBq; room temperature). Probe placement was verified by removal of the brain from the skull and freezing (–20°C). Coronal sections (30 μ m) were made with a cryostat and verified with a stereotactic atlas (21). Animals with probe placements outside the cerebellum or caudate putamen were removed from further analysis. The time–activity curves for both the cerebellum and the caudate putamen were decay-corrected to the time of radiotracer injection. The sensitivity of the 2 probes, as measured with ^{18}F -FDG, was used to convert counts

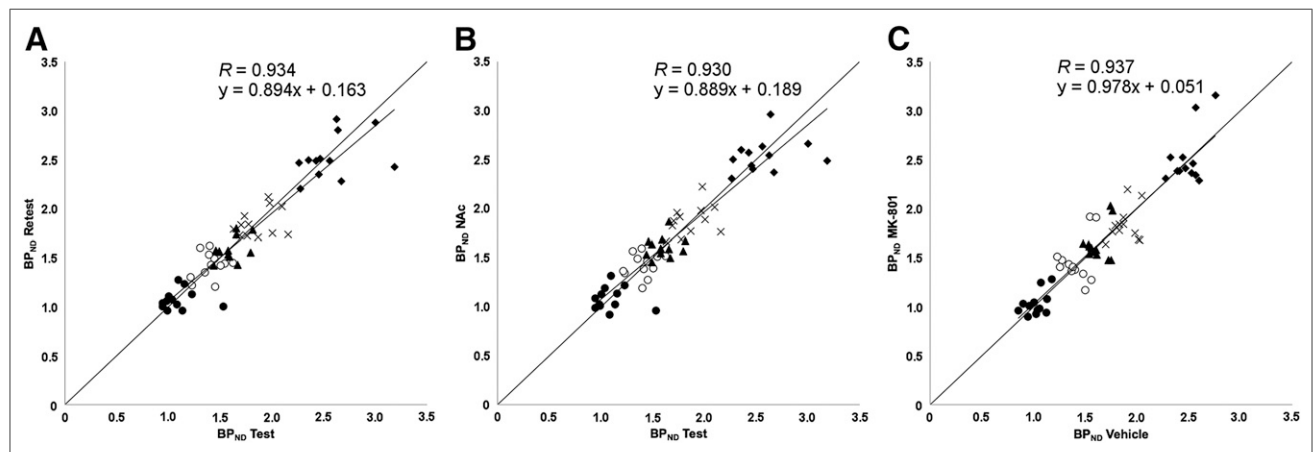


FIGURE 2. Scatterplots for ^{11}C -ABP688 small-animal PET BP_{ND} s for test–retest scans (A), test–NAc challenge (B), and vehicle–MK-801 challenge (C) ($n = 12$ /study). Studied regions were caudate putamen (\blacklozenge), frontal cortex (\circ), cerebral cortex (\blacktriangle), hippocampus (\times), and thalamus (\bullet).

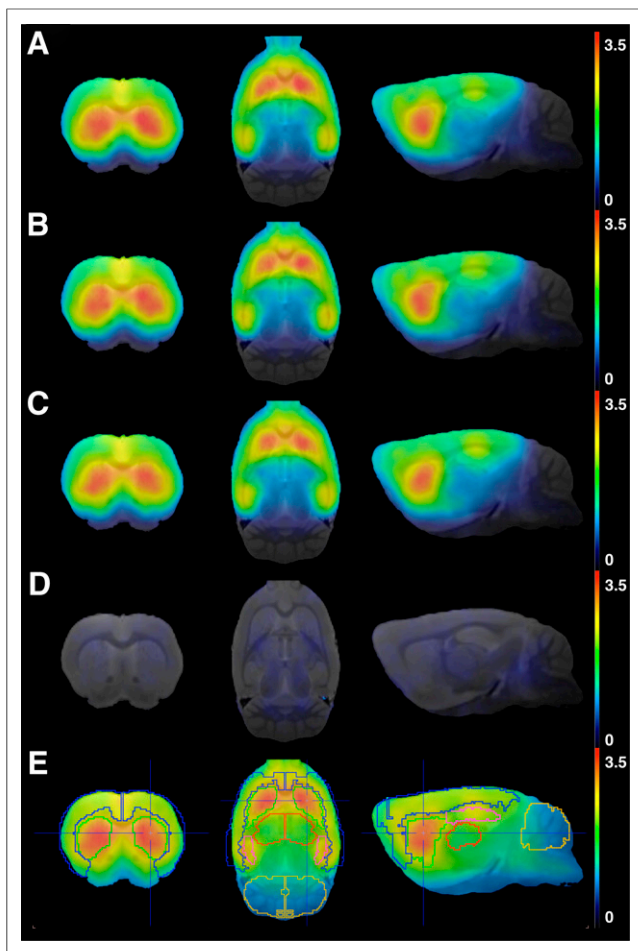


FIGURE 3. (A–D) Illustrations of averaged ^{11}C -ABP688 BP_{ND} images after test (A), NAc (B), MK-801 (C), and unlabeled ABP688 (D) challenges. (E) VOI template (PMOD v3.3) with 5 relevant brain areas (cerebellum [yellow], cerebral cortex [blue], caudate putamen [green], thalamus [red], and hippocampus [pink]) is overlaid on ^{11}C -ABP688 template.

per second into radioactive concentrations (kBq/mL) (PMOD v3.3 SAMPLE) (23). The BP_{ND} of ^{11}C -ABP688 in the caudate putamen was determined by use of the simplified reference tissue model with the cerebellum as a reference region.

Statistical Analysis

BP_{ND} data are expressed as mean \pm SD. Statistical comparisons of the small-animal PET datasets were performed with the Wilcoxon signed rank test. For β -microprobe measurements, a Mann–Whitney U test was performed (SPSS20; SPSS Inc.). The α test level was set to 0.05.

RESULTS

Validation of Experimental Setup

With regard to validation of the extraction procedure and the stability of the tracer, radio-HPLC analysis of the supernatant of spiked plasma and brain samples revealed no degradation of the tracer and no formation of a (*Z*)-isomer during work-up. For plasma, an extraction efficiency of 89.84% (SD, 1.99%) was obtained. For the brain, homogenization with 2 mL of ACN resulted in an extraction efficiency of 77.98%. The extraction efficiencies obtained for plasma and the brain indicated low levels of protein binding of the tracer. After *in vivo* metabolism, only 1 polar metabolite was present in the brain and 2 polar metabo-

lites were present in the plasma at 60 min after tracer injection. In the rat brain, 81.28% (SD, 4.27%) of the intact tracer remained, whereas in rat plasma, 21.85% (SD, 12.10%) of the intact tracer remained. No isomerization of (*E*)- ^{11}C -ABP688 to (*Z*)- ^{11}C -ABP688 could be detected. Comparable metabolite profiles were obtained for rats treated with MK-801 as a selected therapy; only 1 polar metabolite was present in the brain and 2 polar metabolites were present in the plasma at 60 min after tracer injection. In rats treated with MK-801, 76.95% (SD, 7.62%) and 5.96% (SD, 0.46%) of the intact tracer remained in the brain and plasma, respectively. In addition, after treatment, no isomerization of (*E*)- ^{11}C -ABP688 to (*Z*)- ^{11}C -ABP688 could be detected.

With regard to the test–retest small-animal PET data, both the test BP_{ND} and the retest BP_{ND} for the caudate putamen, cerebral cortex, frontal cortex, hippocampus, and thalamus, calculated by use of the simplified reference tissue model with the cerebellum as a reference, are summarized in Table 2 and Figure 2. The absolute percentage changes across the test–retest condition were determined (Table 2; Fig. 3) to be 0.6% (SD, 9.9%) to 2.0% (SD, 10.7%). Accordingly, no significant changes in BP_{ND} across the test–retest condition were found in any of the tested regions. The Pearson correlation coefficient for test BP_{ND} and retest BP_{ND} was 0.934 (Fig. 2).

In the small-animal PET blocking experiment, the average BP_{ND} values in 5 relevant brain areas with various amounts of unlabeled ABP688 (0.00077 [vehicle], 0.003, 0.0098, 0.018, 0.085, 0.84, and 3 mg/kg) were determined (Figs. 3 and 4). A reduction in BP_{ND} was observed with increasing amounts of unlabeled ABP688.

In the β -microprobe blocking experiment, because β -microprobe surgery was end-of-life surgery, a test–retest procedure was not feasible. We determined the average BP_{ND} to be 0.59 (SD, 0.21) in a test (vehicle) experiment, and we measured an average BP_{ND} of only 0.13 (SD, 0.12) in the caudate putamen after blocking with the largest amount of unlabeled ABP688 used (3 mg/kg).

Response to Pharmacologically Induced Glutamate Changes

First, for the 3 challenge conditions (test, retest, and NAc), we calculated the average BP_{ND} values in 5 relevant brain areas on small-animal PET as well as the absolute percentage changes across the test–NAc condition (Table 2; Fig. 2). The BP_{ND} values for these conditions were not significantly different. The Pearson correlation coefficient for the BP_{ND} in the test condition and the BP_{ND} in the NAc condition was 0.930 (Fig. 2).

Second, for the small-animal PET results with an MK-801 challenge, we performed an additional test experiment because the vehicle was given intraperitoneally, as needed for MK-801, instead of as an infusion, as needed for NAc. For the 2 conditions (vehicle and MK-801), we again calculated the average BP_{ND} values in 5 relevant brain areas as well as the percentage changes across the test–MK-801 condition (Table 3; Fig. 2). None of the BP_{ND} values for these conditions were significantly different ($R = 0.937$) (Figs. 2 and 3). As an additional verification, time–activity curves normalized to the sum over all time points of the average activity in the cerebellum for the vehicle and MK-801 conditions are shown in Figure 5. The time–activity curves did not differ significantly.

As an additional validation, we repeated the MK-801 experiment with β -microprobes. Histology showed correct positioning of the β -microprobes in all 20 rats. The average BP_{ND} for the vehicle-injected animals was 0.94 (SD, 0.35); the average BP_{ND} for the MK-801-injected animals—0.76 (SD, 0.23)—was lower, but not significantly so ($P = 0.384$). Normalized time–activity curves in

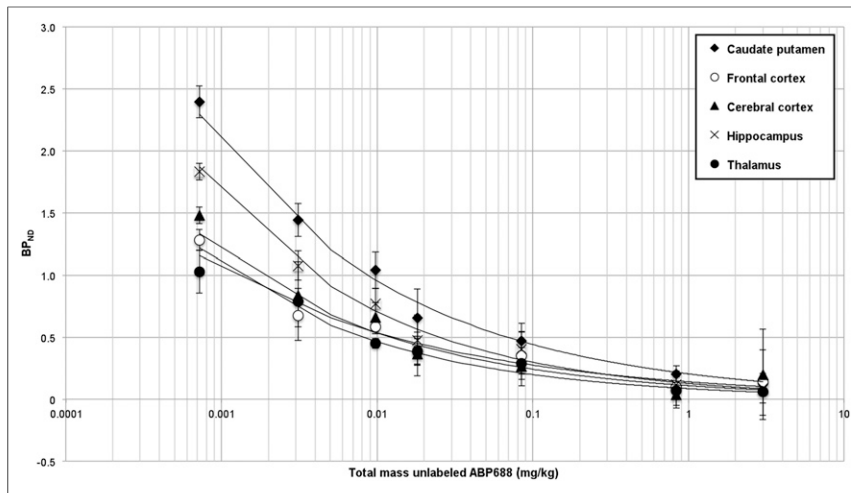


FIGURE 4. BP_{ND} of ^{11}C -ABP688 binding (small-animal PET) after pretreatment with different masses of unlabeled ABP688.

the vehicle and MK-801 challenges also did not differ significantly (Fig. 5). No correlation between the location of the β -microprobes in the caudate putamen and the BP_{ND} was found.

DISCUSSION

The present study did not reveal any change in in vivo ^{11}C -ABP688 binding in the rat brain after pharmacologic challenge with NAc or MK-801, as measured with small-animal PET or with β -microprobes. The experimental setup was validated, and in an in vivo metabolite analysis, we found that more than 76% of the intact tracer remained in the brain at 60 min after tracer injection and that no isomerization of (*E*)- ^{11}C -ABP688 to (*Z*)- ^{11}C -ABP688 occurred in plasma or in the brain. Further, the small-animal PET test–retest data indicated that the ^{11}C -ABP688 tracer bound specifically and stably in delineated structures of the rat brain, such as the caudate putamen, cerebral cortex, frontal cortex, hippocampus, and thalamus, with BP_{ND} s correlating closely with those in the literature (8,9). A human ^{11}C -ABP688 test–retest study recently revealed higher binding in the retest condition than in the test condition, and this finding could not be attributed to injected mass, dose, or clearance (24). The origin of this finding remains to be elucidated because, in our own rat study as well as in previous rat (9), baboon (4,25), and rhesus monkey (26) studies, stable test–retest results with low within-subject variability were observed.

Blocking experiments in which pretreatment with unlabeled ABP688 was used confirmed the capacity of both small-animal PET and β -microprobes to discriminate changes in ^{11}C -ABP688

binding. On the basis of these blocking experiments and literature findings (9), we chose to keep the injected mass of ^{11}C -ABP688 at less than 3 nmol/kg. With this mass, stable test–retest results were obtained, and low intraanimal variations in terms of injected mass were introduced; these data strengthened the finding that our procedure was sensitive enough to detect subtle changes in the BP_{ND} of ^{11}C -ABP688.

Next, the response of ^{11}C -ABP688 binding to pharmacologic treatment with NAc or MK-801 was evaluated. Both compounds are known to induce changes in endogenous extraneuronal glutamate levels (7,27). Small-animal PET experiments revealed no significant changes in BP_{ND} in the test, retest, NAc, vehicle (MK-801), and MK-801 pretreatment conditions

for any of the relevant brain regions. Although PET scanners have been successfully miniaturized for use in small animals, the spatial resolution of small-animal PET systems currently in use is about 1.4 mm at the center of the field of view (13). Further, because of spillover and partial-volume effects, quantification of subtle changes in the binding of ^{11}C -ABP688 in small VOIs can be challenging. Therefore, additional pharmacologic challenge experiments with β -microprobes stereotactically implanted in the caudate putamen and cerebellum were performed. β -microprobes have the advantage of detecting the radiotracer within a small volume around the tip of the probe (10). The β -microprobe experiments confirmed the small-animal PET findings, and no significant changes in BP_{ND} in the vehicle and MK-801 pretreatment conditions were observed. Our experiments thus demonstrated that the mGluR5 radiotracer ^{11}C -ABP688 was not able to discriminate changes in endogenous glutamate levels induced by NAc or MK-801 in the rat brain in vivo. Although glutamate binds to an orthosteric site of mGluR5, the ^{11}C -ABP688 radiotracer is known to bind to an allosteric site of this receptor. Thus, our findings indicated that the increased levels of endogenous glutamate induced by the administration of NAc or MK-801 did not alter the capacity of mGluR5 for binding to ^{11}C -ABP688 in the rat brain.

The NAc dosage used in the present study (50 mg/kg/h; continuous 1 h intravenous infusion) was reported to be high enough to induce significant increases in extracellular glutamate levels, as measured in vivo with microdialysis in the rat brain (28). The intraperitoneal MK-801 dosage used in the present study (0.16

TABLE 3
 BP_{ND} and ΔBP_{ND} for Vehicle and MK-801 Challenges in ^{11}C -ABP688 Small-Animal PET

| Region | Mean \pm SD | | |
|-----------------|-------------------|------------------|---------------------------------|
| | Vehicle BP_{ND} | MK-801 BP_{ND} | Vehicle–MK-801 ΔBP_{ND} |
| Caudate putamen | 2.49 \pm 0.13 | 2.51 \pm 0.28 | 0.6% \pm 8.8% |
| Frontal cortex | 1.41 \pm 0.13 | 1.46 \pm 0.23 | 3.1% \pm 15.3% |
| Cerebral cortex | 1.62 \pm 0.10 | 1.64 \pm 0.18 | 1.0% \pm 9.9% |
| Hippocampus | 1.88 \pm 0.11 | 1.83 \pm 0.17 | –2.9% \pm 9.4% |
| Thalamus | 1.03 \pm 0.06 | 1.03 \pm 0.12 | 0.7% \pm 10.6% |

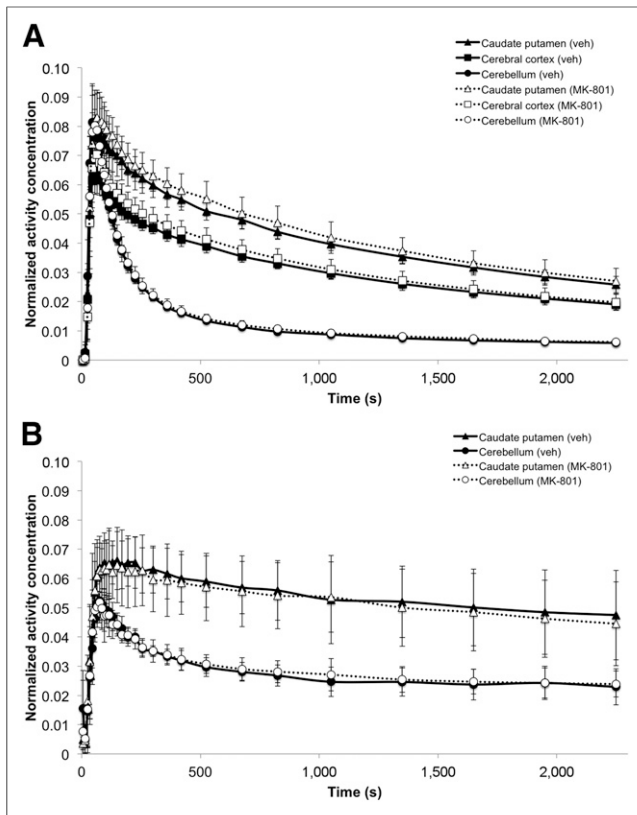


FIGURE 5. Time-activity curves for ^{11}C -ABP688 small-animal PET ($n = 12$; scanned for both conditions) (A) and ^{11}C -ABP688 β -microprobe measurements ($n = 10/\text{condition}$) (B) after vehicle (veh) and MK-801 pretreatments, normalized for total cerebellar count.

mg/kg) was also reported to be high enough to induce increases in glutamate levels (11). Both NAC and MK-801 increased glutamate levels, although through fundamentally different mechanisms. NAC is converted to cystine, a substrate for the glutamate-cystine antiporter, preferentially expressed on glia. This antiporter allows for the uptake of cystine, which causes the reverse transport of glutamate into the extracellular space (6,7). Therefore, it is presumed that NAC administration directly regulates the amount of glutamate present in the extracellular space. On the other hand, MK-801 is a potent NMDA receptor antagonist (27,29). Besides its effect on increasing glutamate levels through the antagonism of NMDA receptors, MK-801 may also directly influence mGluR5 functional status because there is evidence that mGluR5 and NMDA receptors functionally interact; the activation of mGluR5 potentiates NMDA receptor currents, and NMDA receptor activation potentiates mGluR5-mediated responses (30,31). These data indicate that neither increased glutamate levels nor a change in the functional status of mGluR5 through inhibition of the NMDA receptor affects the binding of ^{11}C -ABP688. We conclude that ^{11}C -ABP688 is not a suitable radiotracer for measuring acute fluctuations in extraneuronal levels of glutamate in vivo in the rat brain; rather, this radiotracer can be used to measure differences in mGluR5 density or occupancy of the allosteric site of mGluR5.

In contrast to our results, a recent small-scale study of baboons indicated that ^{11}C -ABP688 was able to visualize acute fluctuations in endogenous glutamate levels after a challenge with NAC (50 mg/kg/h; continuous 1 h intravenous infusion) (4). The discrepancy between our findings and those in the baboon study could be

clarified by the notion that the presumed decrease in BP_{ND} in the NAC experiment (relative to the baseline experiment) in the baboon study might not have been an absolute decrease but rather might have been a relative decrease (compared with the baseline BP_{ND}); counterintuitively, the baseline BP_{ND} was up to 27.4% higher than the test and retest BP_{ND} s in that study. Interestingly, our findings were also confirmed in a recent study with rhesus monkeys (26); in that study, the authors were also unable to reproduce the findings from the baboon study (4). Furthermore, species differences and small differences in methodology might have contributed to the different findings in the present study of rats and the study of baboons (4).

In the present study, ^{11}C -ABP688 binding was measured with both small-animal PET and β -microprobes. These experimental techniques provided the same conclusions but, remarkably, the BP_{ND} s measured in the caudate putamen with the β -microprobes were smaller than the BP_{ND} s measured with small-animal PET. Such a large discrepancy between β -microprobe BP_{ND} s and small-animal PET BP_{ND} s has been described in the literature and can be attributed to changes in the permeability of the blood-brain barrier, blood flow, or local metabolism caused by probe implantation (23,32). We anticipate, however, that this is caused by the low sensitivity of the β -microprobe, which results in count rates barely above the background level because we kept the injected mass dose at around 3 nmol/kg (33) to ensure the same tracer concentrations as in the PET experiment. In addition, a study investigating the impact of unilateral microdialysis probe implantation on tracer binding revealed reduced uptake of ^{18}F -FDG after implantation, an effect that lasted for more than 500 h after implantation (34).

CONCLUSION

The present study showed that the ^{11}C -ABP688 radiotracer was able to specifically and stably bind to delineated structures in the rat brain. However, neither increased glutamate levels after NAC or MK-801 challenge nor a change in the functional status of mGluR5 through inhibition of the NMDA receptor after MK-801 challenge could affect the affinity of mGluR5 for binding to ^{11}C -ABP688, as we demonstrated in vivo with both small-animal PET and β -microprobe measurements in the rat brain.

DISCLOSURE

The costs of publication of this article were defrayed in part by the payment of page charges. Therefore, and solely to indicate this fact, this article is hereby marked "advertisement" in accordance with 18 USC section 1734. No potential conflict of interest relevant to this article was reported.

REFERENCES

- Bradford HF. Glutamate, GABA and epilepsy. *Prog Neurobiol.* 1995;47:477-511.
- Olney JW, Farber NB. Glutamate receptor dysfunction and schizophrenia. *Arch Gen Psychiatry.* 1995;52:998-1007.
- Chase TN, Oh JD. Striatal dopamine- and glutamate-mediated dysregulation in experimental parkinsonism. *Trends Neurosci.* 2000;23(suppl):S86-S91.
- Miyake N, Skinbjerg M, Easwaramoorthy B, et al. Imaging changes in glutamate transmission in vivo with the metabotropic glutamate receptor 5 tracer [^{11}C] ABP688 and *N*-acetylcysteine challenge. *Biol Psychiatry.* 2011;69:822-824.
- Ametamey SM, Kessler LJ, Honer M, et al. Radiosynthesis and preclinical evaluation of ^{11}C -ABP688 as a probe for imaging the metabotropic glutamate receptor subtype 5. *J Nucl Med.* 2006;47:698-705.

6. Dean O, Giorlando F, Berk M. *N*-acetylcysteine in psychiatry: current therapeutic evidence and potential mechanisms of action. *J Psychiatry Neurosci*. 2011;36:78–86.
7. Dean OM, Bush AI, Berk M. Translating the Rosetta Stone of *N*-acetylcysteine. *Biol Psychiatry*. 2012;71:935–936.
8. Elmenhorst D, Minuzzi L, Aliaga A, et al. In vivo and in vitro validation of reference tissue models for the mGluR(5) ligand [¹¹C]ABP688. *J Cereb Blood Flow Metab*. 2010;30:1538–1549.
9. Elmenhorst D, Aliaga A, Bauer A, Rosa-Neto P. Test-retest stability of cerebral mGluR5 quantification using [¹¹C]ABP688 and positron emission tomography in rats. *Synapse*. 2012;66:552–560.
10. Daghighian F, Mazziotta JC, Hoffman EJ, et al. Intraoperative beta probe: a device for detecting tissue labeled with positron or electron emitting isotopes during surgery. *Med Phys*. 1994;21:153–157.
11. Léna I, Chessel A, Le Pen G, Krebs M-O, Garcia R. Alterations in prefrontal glutamatergic and noradrenergic systems following MK-801 administration in rats prenatally exposed to methylazoxymethanol at gestational day 17. *Psychopharmacology (Berl)*. 2007;192:373–383.
12. Wyss MT, Ametamey SM, Treyer V, et al. Quantitative evaluation of ¹¹C-ABP688 as PET ligand for the measurement of the metabotropic glutamate receptor subtype 5 using autoradiographic studies and a beta-scintillator. *Neuroimage*. 2007;35:1086–1092.
13. Visser EP, Disselhorst JA, Brom M, et al. Spatial resolution and sensitivity of the Inveon small-animal PET scanner. *J Nucl Med*. 2009;50:139–147.
14. Bao Q, Newport D, Chen M, Stout DB, Chatziioannou AF. Performance evaluation of the Inveon dedicated PET preclinical tomograph based on the NEMA NU-4 standards. *J Nucl Med*. 2009;50:401–408.
15. Constantinescu CC, Mukherjee J. Performance evaluation of an Inveon PET preclinical scanner. *Phys Med Biol*. 2009;54:2885–2899.
16. Hudson HM, Larkin R. Accelerated image reconstruction using ordered subsets of projection data. *IEEE Trans Med Imaging*. 1994;13:601–609.
17. Defrise M, Kinahan P, Townsend D, Michel C, Sibomana M, Newport D. Exact and approximate rebinning algorithms for 3-D PET data. *IEEE Trans Med Imaging*. 1997;16:145–158.
18. Watson CC. New, faster, image-based scatter correction for 3D PET. *IEEE Trans Nucl Sci*. 2000;47:1587–1594.
19. Lammertsma AA, Hume SP. Simplified reference tissue model for PET receptor studies. *Neuroimage*. 1996;4:153–158.
20. Pain F, Dhenain M, Gurden H, et al. A method based on Monte Carlo simulations and voxelized anatomical atlases to evaluate and correct uncertainties on radio-tracer accumulation quantitation in beta microprobe studies in the rat brain. *Phys Med Biol*. 2008;53:5385–5404.
21. Paxinos G, Watson C. *The Rat Brain in Stereotaxic Coordinates*. San Diego, CA: Academic Press; 2007.
22. Weber B, Späth N, Wyss M, et al. Quantitative cerebral blood flow measurements in the rat using a beta-probe and H₂¹⁵O. *J Cereb Blood Flow Metab*. 2003;23:1455–1460.
23. Ginovart N, Sun W, Wilson AA, Houle S, Kapur S. Quantitative validation of an intracerebral beta-sensitive microprobe system to determine in vivo drug-induced receptor occupancy using [¹¹C]raclopride in rats. *Synapse*. 2004;52:89–99.
24. DeLorenzo C, Kumar J, Mann J, Parsey R. In vivo variation in metabotropic glutamate receptor subtype 5 binding using positron emission tomography and [¹¹C]ABP688. *J Cereb Blood Flow Metab*. 2011;31:2169–2180.
25. DeLorenzo C, Milak M, Brennan K, Kumar J, Mann J, Parsey R. In vivo positron emission tomography imaging with [¹¹C]ABP688: binding variability and specificity for the metabotropic glutamate receptor subtype 5 in baboons. *Eur J Nucl Med Mol Imaging*. 2011;38:1083–1094.
26. Sandiego CM, Nabulsi N, Lin SF, et al. Studies of the metabotropic glutamate receptor 5 radioligand [¹¹C]ABP688 with *N*-acetylcysteine challenge in rhesus monkeys. *Synapse*. 2013;67:489–501.
27. Kovacic P, Somanathan R. Clinical physiology and mechanism of dizocilpine (MK-801): electron transfer, radicals, redox metabolites and bioactivity. *Oxid Med Cell Longev*. 2010;3:13–22.
28. Baker DA, McFarland K, Lake RW, Shen H, Toda S, Kalivas PW. *N*-acetylcysteine-induced blockade of cocaine-induced reinstatement. *Ann N Y Acad Sci*. 2003;1003:349–351.
29. Andiné P, Widermark N, Axelsson R, et al. Characterization of MK-801-induced behavior as a putative rat model of psychosis. *J Pharmacol Exp Ther*. 1999;290:1393–1408.
30. Alagarsamy S, Marino MJ, Rouse ST, Gereau RW, Heinemann SF, Conn PJ. Activation of NMDA receptors reverses desensitization of mGluR5 in native and recombinant systems. *Nat Neurosci*. 1999;2:234–240.
31. Homayoun H, Moghaddam B. Bursting of prefrontal cortex neurons in awake rats is regulated by metabotropic glutamate 5 (mGlu5) receptors: rate-dependent influence and interaction with NMDA receptors. *Cereb Cortex*. 2006;16:93–105.
32. Myers RD, Adell A, Lankford MF. Simultaneous comparison of cerebral dialysis and push-pull perfusion in the brain of rats: a critical review. *Neurosci Biobehav Rev*. 1998;22:371–387.
33. Hume SP, Gunn RN, Jones T. Pharmacological constraints associated with positron emission tomographic scanning of small laboratory animals. *Eur J Nucl Med*. 1998;25:173–176.
34. Schiffer WK, Mirrione MM, Biegone A, Alexoff DL, Patel V, Dewey SL. Serial microPET measures of the metabolic reaction to a microdialysis probe implant. *J Neurosci Methods*. 2006;155:272–284.